

## Local structural distortions in manganites probed by comparative x-ray-emission and x-ray-absorption near-edge measurements

Q. Qian,<sup>1</sup> T. A. Tyson,<sup>1</sup> C.-C. Kao,<sup>2</sup> M. Croft,<sup>3</sup> S.-W. Cheong,<sup>3</sup> G. Popov,<sup>4</sup> and M. Greenblatt<sup>4</sup>

<sup>1</sup>*Department of Physics, New Jersey Institute of Technology, Newark, New Jersey 07102*

<sup>2</sup>*Brookhaven National Laboratory, Upton, New York 11973*

<sup>3</sup>*Department of Physics and Astronomy, Rutgers University, Piscataway, New Jersey 08854*

<sup>4</sup>*Department of Chemistry, Rutgers University, Piscataway, New Jersey 08854*

(Received 6 July 2000; revised manuscript received 25 January 2001; published 22 June 2001)

Comparison studies of the perovskite compounds system  $R_{1-x}\text{Ca}_x\text{MnO}_3$  ( $R=\text{La, Bi}$ ) by both Mn  $K_{\beta}$ -emission spectroscopy and x-ray-absorption near-edge spectroscopy (XANES) are presented. The insensitivity of x-ray-emission measurements to structural distortions coupled with the sensitivity of x-ray-absorption near-edge measurements to changes in both structure and valence enable one to detect the presence of structural distortions, such as local Jahn-Teller (JT) distortions. Theoretical XANES computations for pure cubic perovskite and locally distorted endmembers are used to show the effect of distortions on XANES spectra as well as to comment on the nature of the pre-edge features in the spectra. We show by explicit computations that the near-edge spectra are determined by dipole transitions while pure  $1s$  to  $3d$  electric quadrupole transitions determine a very limited section of the pre-edge region. Simulations of the pre-edge features reveal a direct connection between local distortions and the  $a1$  feature amplitude. The Bi-containing system is found to have significantly higher levels of distortions than the La system. XANES studies of the  $A\text{MnO}_3$  ( $A=\text{La, Pr, and Nd}$ ) system reveal a direct relationship between the main line width and the magnitude of the JT distortions.

DOI: 10.1103/PhysRevB.64.024430

PACS number(s): 78.70.En, 61.10.Ht, 78.70.Dm, 75.70.Pa

### I. INTRODUCTION

Interest in orbital ordering, charge ordering, and Jahn-Teller (JT) distortions in the manganite system  $T_{1-x}D_x\text{MnO}_3$  ( $T$ =trivalent cation,  $D$ =divalent cation) was kindled recently due to experiments by Murakami *et al.*<sup>1</sup> It was claimed that by tuning across the Mn  $K$ -edge in resonant inelastic scattering, one is able to probe directly the orbital and charge ordering. Based on an atomic model of the Mn  $K$ -edge x-ray-absorption spectra, they argued that the Mn  $4p$  levels were split by orbital ordering of the Mn  $e_g$  orbitals. More recent band structure computations (LSDA+U) have revealed that the spin-polarization dependence of the  $K$ -edge absorption cross section (obtained from the density of states) is determined by band structure effects rather than by local Coulomb interactions.<sup>2</sup> Moreover, polarized full multiple scattering computations show that JT distortions are the primary producers of the polarization dependent splitting of the main line.<sup>3</sup> Hence the electronic and structural changes in the Mn  $K$  edges of manganites as a function of cation type and  $x$ , may reveal fundamental structural and electronic properties of these materials. Consequently, a thorough study of the absorption edges is necessary in order to properly assess the origin of the observed features. The question of whether the main absorption line is atomic in origin or if a band picture is relevant must be addressed.

In the past, many workers have attempted to explain the complex phase diagrams from the perspective of linear combinations of the endmember compounds. Park *et al.*,<sup>4</sup> based on Mn  $2p$  x-ray-photoemission spectrum (XPES) and O  $1s$  absorption, support the double exchange theory with mixed valence  $\text{Mn}^{3+}/\text{Mn}^{4+}$  ion. They were able to obtain approxi-

mate spectra of the intermediate doping XPES spectra by linearly combining the end-member spectra—consistent with a linear change of spectral features with doping. However, the significant discrepancy between the weighted spectrum and the prepared spectrum (for given  $x$ ) suggests a more complex doping effect. Subias *et al.*<sup>5</sup> examined the valence state of Mn utilizing Mn  $K$ -edge x-ray-absorption near-edge spectroscopy (XANES). Again, a large discrepancy is found between intermediate doping spectra and linear combinations of the end members. They suggest that Mn does not fluctuate between  $3+$  and  $4+$  (not ionic) and find a unique magnetic signature for Mn using x-ray magnetic dichroism measurements. Systematic shifts in the absorption edge position with doping have been found by Subias *et al.* (Mn  $K$  edge),<sup>5</sup> Booth *et al.* (Mn  $K$  edge),<sup>6</sup> Croft *et al.* (Mn  $K$  edge),<sup>7</sup> Liu *et al.* (Mn  $L$  edge), and Pellegrin *et al.* (Mn  $L$  edge and O  $K$  edge).<sup>8</sup>

Mn  $K_{\beta}$ -emission spectroscopy (XES) provides a direct method to probe the total Mn  $3d$  spin  $S$  and effective charge density (and valence) on the Mn sites as has been shown in our previous work on the manganites.<sup>9</sup> The main line position and satellite to main line ratios depend both on the oxidation and the spin state of Mn. The details of the multiplet structure depend on the  $3d$  spin alignment (high spin vs low spin) and point group symmetry of the Mn site (crystal field effects) to a lesser extent.<sup>10–12</sup> XANES spectra (as will be seen in detail below) are determined by both the local structural arrangement about the Mn site and by the valence of Mn site. Hence, the combined measurements can be used to ascertain differences in both the valence and structure in manganite systems with different cations (La and Bi).

In order to understand the trends in valence and local structure of manganites, we have performed complementary

Mn  $K_\beta$  emission and x-ray-absorption near-edge measurements of the distinctly different manganite systems  $\text{La}_{1-x}\text{Ca}_x\text{MnO}_3$  (La/Ca) and  $\text{Bi}_{1-x}\text{Ca}_x\text{MnO}_3$  (Bi/Ca). We have found that reduction in the amplitudes (and enhancement of the width) of the main lines in XANES are due to the presence of structural distortions, suggesting that the main line intensity profiles can be used as indicators of distortions in these materials. Furthermore, we compare the XANES spectra of  $\text{AMnO}_{3+\delta}$  ( $A = \text{La}, \text{Pr}, \text{and Nd}$ ) for varying O content where the magnitude of the JT distortion is known to vary systematically. In these materials, the main-line profile is a direct mirror of the degree of JT distortion.

## II. EXPERIMENTAL AND THEORETICAL METHODS

Samples of  $\text{La}_{1-x}\text{Ca}_x\text{MnO}_3$ ,  $\text{Bi}_{1-x}\text{Ca}_x\text{MnO}_3$ ,  $\text{PrMnO}_3$ , and  $\text{NdMnO}_3$  were synthesized and characterized as described by the standard solid-state method (Ref. 7 for  $\text{La}_{1-x}\text{Ca}_x\text{MnO}_3$ ).  $\text{La}_{1-x}\text{Ca}_x\text{MnO}_3$  displays the well known complex  $x$  dependent phase diagram while  $\text{Bi}_{1-x}\text{Ca}_x\text{MnO}_3$  ( $x \geq 0.4$ ) is antiferromagnetic and insulating except near  $x = 0.875$  where the net moment on the average Mn site approaches 1 Bohr magneton (canted spins).<sup>13</sup> Powder samples were prepared by methods similar to those used in other studies, for which a large body of transport and magnetic measurement exist in the literature. Fluorescence measurement samples were prepared by finely grinding the materials and brushing the powder onto adhesive tape.

The Mn  $K_\beta$  fluorescence measurements were performed at the National Synchrotron Light Source's (NSLS) 27 pole wiggler Beamline X21A. The experimental setup, which consists of an analyzer and detector in Rowland circle geometry, is described in Ref. 14 and previously published data on the manganite system can be found in Ref. 9.

An incident energy ( $\hbar\omega$ ) of 6556 eV was selected using a four-bounce Si(220) monochromator. The incident energy was calibrated by the known Mn metal  $K$ -edge-absorption inflection point (6539 eV). Five spherically bent Si(220) analyzer crystals were used to resolve the energy of the emitted photons,  $\hbar\Omega$ . A solid-state Biclon fluorescence detector was used to measure the fluorescence radiation. The absolute fluorescence photon energy was calibrated from the elastic scattering peaks of the sample at the same position utilizing the known incident energy. Error bars are determined by assuming a Gaussian distribution in the number of counts at each energy point. The x-ray-absorption spectra were measured at beam line X19A [room temperature in fluorescence mode (Ref. 7)] using Si(111) monochromators (with 1/4 and 1/2 mm vertical slits, respectively) Normalization of the data followed standard procedures.<sup>15</sup>

The theoretical XANES presented here were computed using the RELXAS programs.<sup>16</sup> The spectra were generated in a manner analogous to that of Ref. 17 except that a direct inversion of the scattering matrix was carried out. A complex biconjugate gradient algorithm was used to effect this after the scattering matrix was preconditioned by diagonal scaling (see Ref. 18). The potentials were computed for perovskite structures, based on clusters containing the first 142 atoms surrounding the absorber, obtained using the program

MSCALC.<sup>19</sup> In this way, accurate interstitial and atomic potentials were derived. The XANES spectra were then computed using the muffin-tin potentials from these calculations but including only the atomic potentials from a given number of shells corresponding to 7, 21, 51, and 87 (or 85 for distorted  $\text{LaMnO}_3$ ) atoms, respectively. The maximum  $l$  value was set to 3. In determining the phase shifts, the wave functions were computed with a  $X-\alpha$  exchange and with a Mn core hole width [half width at half maximum (HWHM)] of 0.580 eV added at each point in space. In order to examine the details of the computed spectra no experimental broadening (Gaussian) was included. We note that qualitative improvements can be obtained by utilizing self-consistent potentials in place of the  $Z+1$  approximation used in these calculations. But these improvements do not alter the trends observed here (see Ref. 17, and references therein). The zero of energy given in the computations is not the ionization threshold. Self-consistent field computations are required to define this point in the absorption spectra. Only relative energies between features have meaning. We point out that these calculations are not atomic but include hybridization through the overlap of the potential (charge densities) of neighboring atoms. In the limit of very large cluster size one obtains band structure results.

## III. RESULTS AND DISCUSSION

In order to separate the changes in valence from the changes in structure, we compared x-ray-emission and x-ray-absorption spectra. In Fig. 1(a) we show the  $K_\beta$  emission spectra of  $\text{La}_{1-x}\text{Ca}_x\text{MnO}_3$  as a function of Ca doping. In previous work,<sup>9</sup> the  $\text{La}_{1-x}\text{Ca}_x\text{MnO}_3$  system has been discussed in detail, and it is shown that a spectrum for a given value of  $x$  is a mixture of the end members. Here this doping system is remeasured, and normalized to give the same area under each emission spectrum. (The spectra are normalized to produce a constant emission probability of the Mn  $K_\beta$  lines. This enables quantitative analysis of the transfer of weight between the satellite and main line.) In Fig. 1(b) we show the XANES of the corresponding samples. The absorption edges are systematically shifted.

In Fig. 2(a) we show the  $\text{Bi}_{1-x}\text{Ca}_x\text{MnO}_3$   $K_\beta$  emission spectra over a region in which the system is always insulating. The shifts of the  $K_\beta$  emission spectra are similar to those found in  $\text{La}_{1-x}\text{Ca}_x\text{MnO}_3$ —indicating the same trend in valence in both systems. In Fig. 2(b) we give XANES for this system. Unlike the  $\text{La}_{1-x}\text{Ca}_x\text{MnO}_3$  system we observe significant changes in the shape of the main line  $B$  feature. The main line  $B$ -feature intensity drops significantly at low calcium content. Indeed, extended x-ray-absorption fine-structure measurements on this system reveal that large local structural distortions exist in the low calcium doping range.<sup>20</sup> It is worth noting that the presence of local distortions (ferroelectric or ferrodistorive) in  $\text{ATiO}_3$  ( $A = \text{Ca}, \text{Ba}, \text{Pb}$ ) produce dramatic splittings of the main line  $B$  feature in multiple features.<sup>21</sup>

In Fig. 3 we compare the XES spectra for  $\text{Bi}_{1-x}\text{Ca}_x\text{MnO}_3$  and  $\text{La}_{1-x}\text{Ca}_x\text{MnO}_3$  for  $x = 0.4$  (a) and 0.6 (b). While the XES spectra at higher Ca dopings are similar, for lower Ca

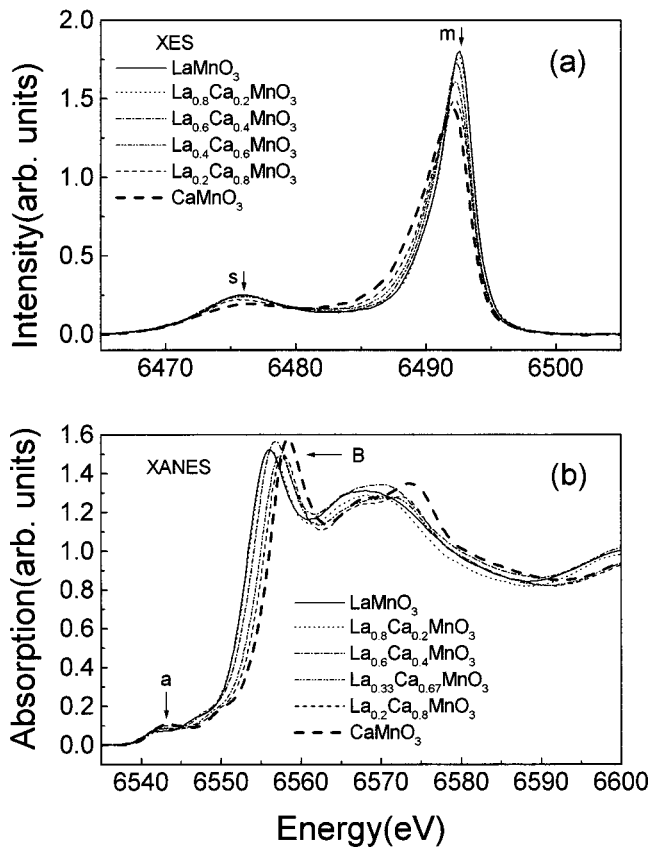


FIG. 1. (a) Mn  $K_{\beta}$  spectra of  $\text{La}_{1-x}\text{Ca}_x\text{MnO}_3$  perovskite system with Ca doping  $x=0, 0.2, 0.4, 0.6, 0.8, 1$ . Note that all spectra are area normalized over the region given. The main line ( $m$ ) and satellite region ( $s$ ) are indicated. (b) Mn  $K$ -edge absorption spectra of  $\text{La}_{1-x}\text{Ca}_x\text{MnO}_3$  with  $x=0, 0.2, 0.4, 0.67, 0.8, 1$ . The main resonance  $B$ -feature and pre-edge  $a$  feature are indicated.

dopings the Bi spectra show shifts in the main line indicative of a difference in covalency (The effects of covalency on XES spectra are discussed in our previous work<sup>9</sup>). The comparison of the XES in Figs. 1(a) and 2(a) reveal that the Mn valence of same doping levels ( $x$ ) in both systems are quite similar. Based on this result, we can focus our discussion on the local structure distortions obtained from XANES spectra, which are sensitive to both of valence change and local distortions.

In order to understand the nature of the changes in the XANES with doping and the origin of the pre-edge features, multiple scattering Mn  $K$ -edge calculation for clusters of various sizes have been performed on  $\text{LaMnO}_3$  and  $\text{CaMnO}_3$ . An ideal perovskite model [cubic with Mn-O bond of 2.018 Å based on the structure of  $\text{CaMnO}_3$  (Ref. 22)] was constructed for  $\text{LaMnO}_3$  and compared with a model based on the known JT-distorted structure<sup>23</sup> (room temperature neutron diffraction data with three pairs of Mn-O bonds at 1.968, 1.907, and 2.178 Å). These model spectra were compared with spectra of the known orthorhombic (but almost cubic) structure of  $\text{CaMnO}_3$  (Ref. 22) (room-temperature neutron diffraction data with three pairs of Mn-O bonds at 1.895, 1.900, and 1.903 Å). The calculations as a function of cluster size (number of atoms about Mn at origin) are shown

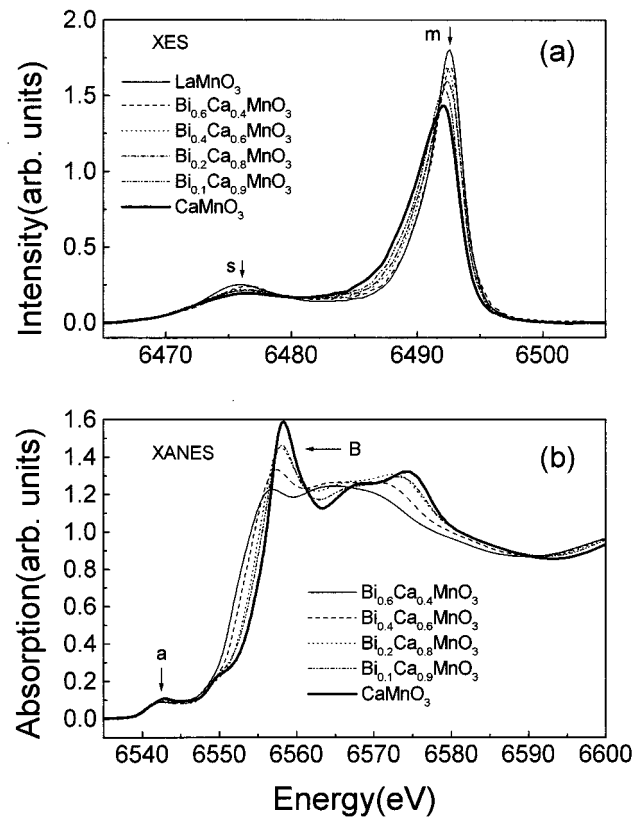


FIG. 2. (a) Mn  $K_{\beta}$  spectra of  $\text{Bi}_{1-x}\text{Ca}_x\text{MnO}_3$  perovskite system with Ca doping  $x=0.4, 0.6, 0.8, 0.9, 1$ , and  $\text{LaMnO}_3$  (b) Mn  $K$ -edge absorption spectra of  $\text{Bi}_{1-x}\text{Ca}_x\text{MnO}_3$  with  $x=0.4, 0.6, 0.8, 0.9, 1$ . Note the similarity in emission spectra of Figs. 1 and 2 but difference in the absorption spectra.

in Figs. 4 and 5 for the dipole transitions. The main lines in the  $\text{LaMnO}_3$  and  $\text{CaMnO}_3$  XANES spectra are determined by clusters of at least 21 (51 with JT distortion) or 51 atoms, respectively. The relative intensity of the  $\text{LaMnO}_3$  to the  $\text{CaMnO}_3$  main line  $B$  feature depends strongly on the level of distortions present. Indeed, the cubic  $\text{LaMnO}_3$  model  $B$  feature is as sharp as that in  $\text{CaMnO}_3$ . The  $\text{LaMnO}_3$  peak intensity is reduced and the peak broadens in the JT-distorted state. The large cluster calculations in Fig. 5 clearly reveals  $B$ -feature broadening of the JT distorted  $\text{LaMnO}_3$  model.<sup>3</sup> Polarized XANES computation performed on  $\text{LaMnO}_3$  by us and others<sup>3</sup> show that three separate  $4p$  state components are associated with the different Mn-O bond distances.

Our model calculations indicate that local structural distortions will lead to broadening and splitting of the main line  $B$  feature. Recall that for the Bi-Ca system, the main line broadening increases with Bi content is extremely strong [Fig. 2(b)]. We associate this strong broadening with the presence of strong local distortions induced by the Bi substitution. The broadening of the main line  $B$  feature of pure  $\text{BiMnO}_3$  (Ref. 20) and the similarity of the XES in the Bi-Ca and La-Ca systems support this association. We note that the pure electric quadrupole intensities in the near edge region [Fig. 5(a) inset, for a 51 atom cluster] are found to be small compared with the dipole transitions.

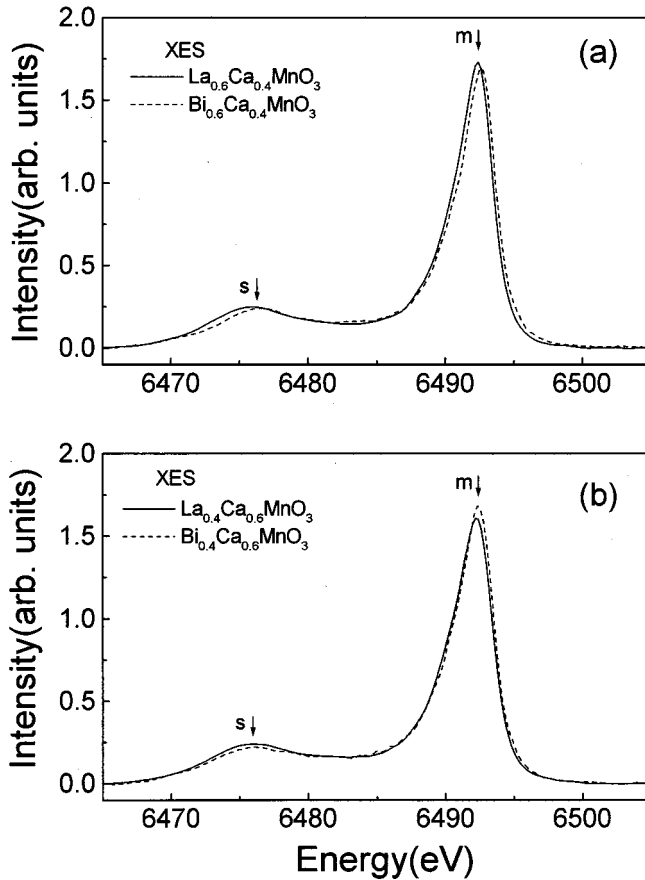


FIG. 3. Comparison XES spectra for  $\text{Bi}_{1-x}\text{Ca}_x\text{MnO}_3$  and  $\text{La}_{1-x}\text{Ca}_x\text{MnO}_3$  for  $x=0.4$  (a) and  $0.6$  (b). While the XES spectra at  $x=0.6$  are similar, the  $x=0.4$  Bi shows shifts in the main line indicative of a difference in covalency.

In Fig. 6 we make direct comparisons of the large cluster dipole transition calculations from Fig. 5(b) with the corresponding experimental data (energy was aligned to XANES main peak). It clearly shows that the major features of the absorption spectra are present in the dipole calculations. While the gross features are well represented, we note that the amplitudes of the features are not well modeled. This is due in part to the limitation of the muffin-tin approximation used as well as the lack of experimental and finite temperature broadening. Note that the states observed in the pre-edge region [Fig. 6(a) inset and Fig. 6(b) inset] require large size clusters for proper treatment indicating they originate from bandlike final states.

A detailed comparison of the calculated pre-edge features to experiment is not possible because of the absence of  $3d$ -correlation effects in the calculation. However, the pre-edge dipole calculation results for the  $e_g$  states (hybridized with  $O$  ligands) features, shown in Fig. 7(a) (energy was aligned to XANES main peak), are worth noting. In the absence of correlations, the  $\text{Mn}-e_g$  band is empty and  $\text{Mn}$  is in a low-spin state. For the undistorted- $\text{LaMnO}_3$  calculation, the dipole- $e_g$ -state absorption is manifested by any single sharp pre-edge peak [see the dashed line in Fig. 7(a)].

In contrast, for the JT- $\text{LaMnO}_3$  calculation, the roughly

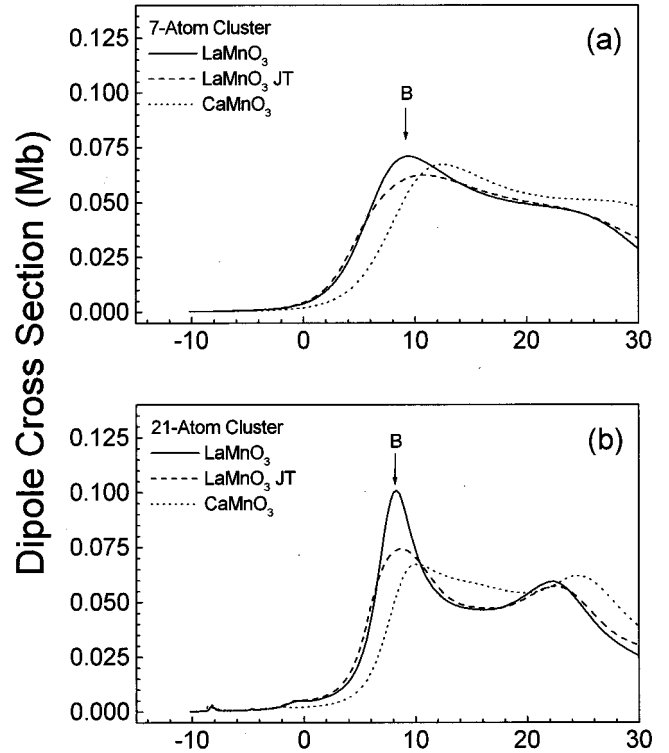


FIG. 4. Mn  $K$ -edge absorption simulations for clusters of varying size. The solid line is ordered  $\text{LaMnO}_3$  (no JT distortion), the dashed line is JT distorted  $\text{LaMnO}_3$  (including JT distortion from diffraction measurements of structure) and the dotted line is  $\text{CaMnO}_3$  (from diffraction measurements of structure). (a) 7 atom cluster model. (b) 21 atom cluster model. Only dipole contributions are considered. Note that the main line is determined by shells beyond the first shell of oxygen atom about Mn. (One Mb is equal  $10^6$  b or  $10^{-18}$   $\text{cm}^2$  and represents the effective cross section.)

0.9 eV, JT splitting of the  $e_g$  feature is dramatically apparent in Fig. 7(a) (solid line). A similar JT splitting of the  $e_g$  states would also occur in a band structure calculation.<sup>24</sup> For qualitative purposes we will therefore use the calculation results in Fig. 7(a) as a guide to the effects that a JT distortion would have in a locally correlated band structure. In the correlated case these  $e_g$  states are spin polarized, partially occupied and the Mn is high spin. This partial occupancy is indicated in Fig. 7(a) by the placement of the Fermi energy ( $E_F - c$ ) in the center of the  $e_g$ -related feature. Here the  $-c$  emphasizes that this is a correlated-case Fermi energy superimposed on an uncorrelated multiple scattering calculation. In the undistorted-metallic case there are empty (high-absorption cross section) states just above  $E_F - c$ . In the JT case the unoccupied state peak is split to higher energy. The down-split JT feature is occupied and cannot contribute to the final state absorption cross section.

In Fig. 7(b) we show the pre-edge features for  $\text{La}_{0.7}\text{Ca}_{0.3}\text{MnO}_3$ : at 300 K, where it is in a local-JT, insulating state; and at 15 K where it is in a metallic state with the JT effect suppressed. The local-JT to metallic change induces a subtle, but reproducible, enhancement in the lowest-energy  $a_1$  pre-edge feature. This enhancement is consistent

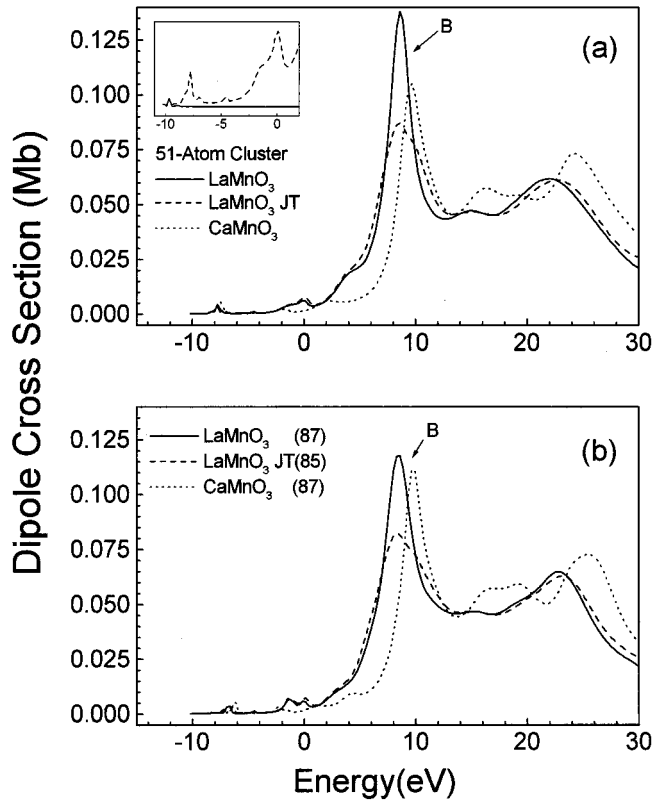


FIG. 5. Mn  $K$ -edge absorption simulations for clusters of varying size. The solid line is ordered  $\text{LaMnO}_3$  (no JT distortion) dashed line is JT distorted  $\text{LaMnO}_3$  and dotted line is  $\text{CaMnO}_3$ . (a) 51 atom cluster model. (b) 85/87 atom cluster model. The inset in (a) shows a calculation for the Mn  $1s$  to  $3d$  quadrupole cross section (solid line) for a 51 atom (JT distorted)  $\text{LaMnO}_3$  cluster compared with the 51 atom (JT distorted) dipole calculation (dashed line). Note that at least three shells are needed to define the main line resonance.

with, the collapse of the JT splitting in the metallic state and the transfer of unoccupied states to  $EF$ - $c$  as seen in our calculation. Thus, our calculation motivates the identification of this pre-edge,  $a1$ -feature enhancement (at 15 K in the metallic phase) as due to the suppression of the JT splitting. Detailed temperature dependent XANES measurements by Bridges *et al.*<sup>25</sup> and combined XANES and XES measurements by our group<sup>26</sup> support our analysis.

The  $\text{Mn}^{3+}$  end members ( $\text{AMnO}_3$ ) are known to exhibit large JT distortions in the  $\text{MnO}_6$  octahedral when prepared by annealing in inert atmospheres while exhibiting significantly reduced distortions when prepared in air (producing  $A$  site defects).<sup>27</sup> To reinforce the effect of JT distortions in XANES spectra, we display the absorption spectra for  $\text{LaMnO}_3$ ,  $\text{PrMnO}_3$ , and  $\text{NdMnO}_3$  annealed in Ar and in air (Fig. 8). Again, note the significant broadening of the main peak which occurs in the JT distorted Ar prepared samples. In addition, the standard deviation of the Mn-O bond lengths from average increases in the series La, Pr, Nd.<sup>28</sup> This is reflected in the widths of the corresponding spectra.

In terms of the sensitivity of the XANES spectra to structural distortions, LSDA+U calculations by Elfimov *et al.*<sup>2</sup>

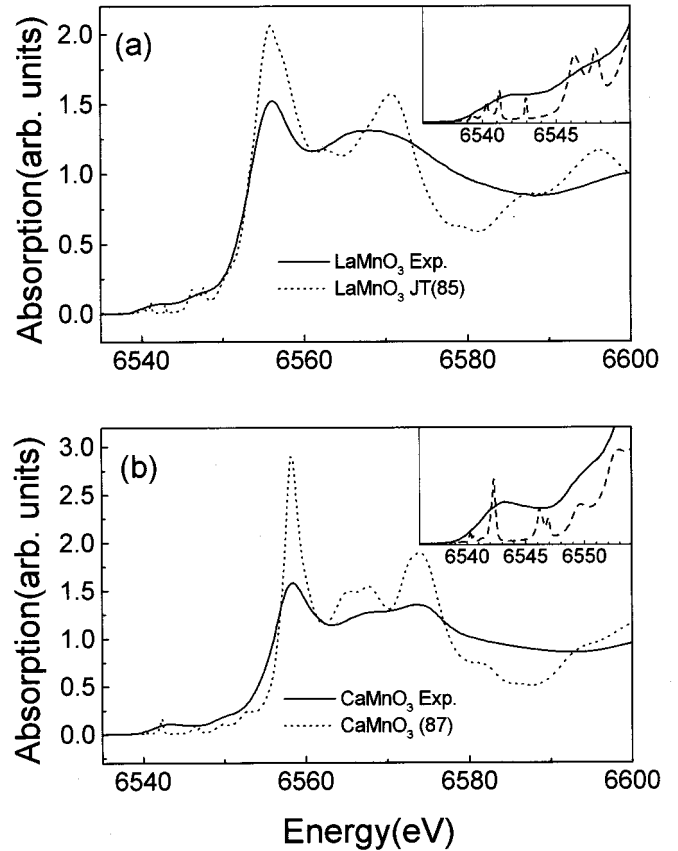


FIG. 6. XANES spectra of  $\text{LaMnO}_3$  and  $\text{CaMnO}_3$  are compared with simulations. (a) The solid line corresponds to  $\text{LaMnO}_3$  experiment data and dotted line corresponds to JT distorted  $\text{LaMnO}_3$  (85 atoms). (b) The solid line corresponds to  $\text{CaMnO}_3$  experiment data and dotted line corresponds to ordered  $\text{CaMnO}_3$  (87 atoms).

reveal that the  $4p$  states on Mn sites hybridize with the  $3d$  states on adjacent Mn sites. Supporting this approach, our calculations show explicitly that, the main line and the pre-edge features are indeed determined by band structure effects—requiring clusters of large size to reproduce their shape. In addition, the dominant  $4p$  level splittings are due to changes in the local Mn-O bond distributions. A band structure approach must be considered in modeling the resonant inelastic scattering in these materials.

The ability to model the XES spectra with weighted endmembers (compared to the XANES spectra) is made clearer. Subias *et al.*<sup>5</sup> showed that at  $x=0.33$  of  $\text{La}_{1-x}\text{Ca}_x\text{MnO}_3$ , the main line of measured spectrum is sharper than the corresponding linear combination of the endmembers. This suggests that the JT distortion as a function of  $x$  fall off faster than a straight line between the endmember distortions.

#### IV. SUMMARY

Comparison studies of the perovskite compounds system  $\text{R}_{1-x}\text{Ca}_x\text{MnO}_3$  ( $R=\text{La, Bi}$ ) by both Mn  $K_\beta$  emission and x-ray-absorption near-edge spectra were presented. The x-ray emission measurements were found to be similar for these two systems, revealing analogous valence changes with

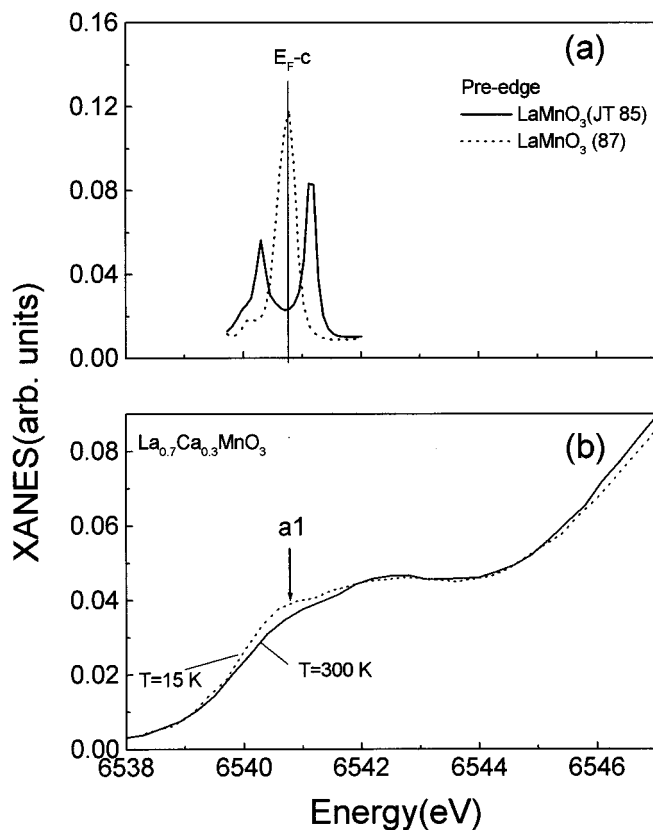


FIG. 7. (a) Cluster model calculation at pre-edge for  $\text{LaMnO}_3$  with JT distortion (85 atoms, solid line) and without JT distortion (87 atoms, dashed line). A vertical line  $E_{F-c}$  put on dashed peak is a Fermi level suspected. (b) Temperature dependent experimental XANES pre-edge spectra of  $\text{La}_{0.7}\text{Ca}_{0.3}\text{MnO}_3$ : solid line (300 K) and dashed line (15 K).

doping ( $x$ ). On the other hand, the XANES spectra of the corresponding Bi and La materials, with the same doping, have quite different shapes—revealing significant local distortions. Thus the combination of XES and XANES allows one to probe the presence of local structural distortions. Theoretical XANES computations for pure cubic and distorted perovskite materials are used to show the effects of local disorder (distortion induced bond distribution) on XANES. The main line amplitude falls and the width increases with enhanced local distortions. We show by explicit computations that the main and pre-edge spectra are determined by dipole transitions while pure  $1s$  to  $3d$  electric quadrupole transitions contribute to a very limited section of the pre-edge region—at much lower energies than previously studied. Simulation of the pre-edge features reveal a direct connection between local distortions and the  $a1$  feature

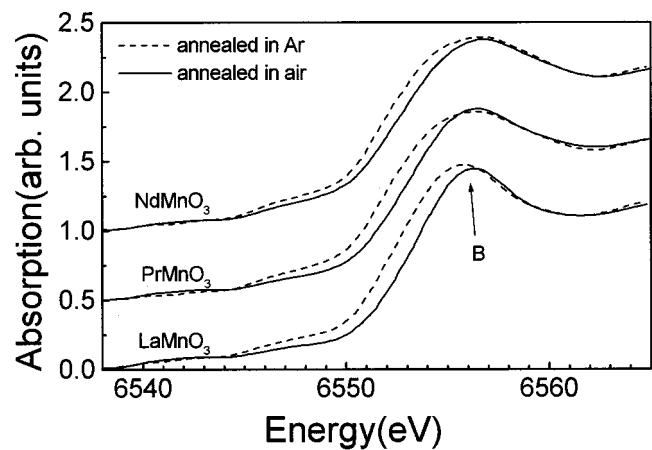


FIG. 8. XANES spectra for the  $\text{Mn}^{3+}$  endmembers  $\text{LaMnO}_3$ ,  $\text{PrMnO}_3$ , and  $\text{NdMnO}_3$  annealed in Ar (dashed line) and in air (solid line) are shown. Sample with large JT distortions exhibit enhanced peak widths.

amplitude. The Bi containing system is found to have significantly higher levels of distortions than the La systems. A systematic measurement of the  $\text{Mn}^{3+}$  end members  $\text{AMnO}_3$  ( $A = \text{La, Pr, and Nd}$ ), reveals a direct relationship between the main line width and the magnitude of local JT distortions as well as the trends in the  $a1$  feature amplitude.

We have shown that JT distortions play a dominant role in determining the shape of the main line Mn  $K$ -edge profile in manganites. However, refined measurements are needed to separate the spin and spatial dependence of the  $K$ -edge spectrum. Spatial and spin polarized Mn  $K$ -edge measurement on single crystals and films are in progress. This additional work may enable a complete decomposition of the absorption spectra and facilitate a direct comparison with bandstructure<sup>2</sup> and cluster computation of the Mn  $p$  partial density of states in these materials.

#### ACKNOWLEDGMENTS

We are indebted to Professor G. A. Sawatzky of the University of Groningen, the Netherlands for insightful discussion. Data acquisition was performed at Brookhaven National Laboratory's National Synchrotron Light Source which is funded by the U.S. Department of Energy. The x-ray measurements were supported by Department of Energy, Office of Basic Energy Sciences Grant No. DE-FG02-97ER45665 and the modeling work was supported by NSF Career Grant No. DMR-9733862. Sample preparation was supported by National Science Foundation Grants No. DMR-93-13106 and DMR-93-14605 (M.G.) and DMR 9802513 (S.W.C.).

<sup>1</sup>Y. Murakami, J. P. Hill, D. Gibbs, M. Blume, I. Koyama, M. Tanaka, H. Kawata, T. Arima, Y. Tokura, K. Hirota, and Y. Endoh, *Phys. Rev. Lett.* **81**, 582 (1998).

<sup>2</sup>I. S. Elfimov, V. I. Anisimov, and G. A. Sawatzky, *Phys. Rev.*

*Lett.* **82**, 4264 (1999).

<sup>3</sup>M. Benfatto, Y. Joly, and C. R. Natoli, *Phys. Rev. Lett.* **83**, 636 (1999).

<sup>4</sup>J.-H. Park, C. T. Chen, S.-W. Cheong, W. Bao, G. Meigs, V.

- Chakarian, and Y. U. Idzerda, *Phys. Rev. Lett.* **76**, 4215 (1996).
- <sup>5</sup>G. Subias, J. Garcia, M. G. Proietti, and J. Blasco, *Phys. Rev. B* **56**, 8183 (1997).
- <sup>6</sup>C. H. Booth, F. Bridges, G. J. Snyder, and T. H. Geballe, *Phys. Rev. B* **54**, 15 606 (1996); C. H. Booth, F. Bridges, G. H. Kwei, J. M. Lawrence, A. L. Cornelius, and J. J. Neumeier, *Phys. Rev. Lett.* **80**, 853 (1998).
- <sup>7</sup>M. Croft, D. Sills, M. Greenblatt, C. Lee, S.-W. Cheong, K. V. Ramanujachary, and D. Tran, *Phys. Rev. B* **55**, 8726 (1997).
- <sup>8</sup>R. S. Liu, J. B. Wu, C. Y. Chang, J. G. Lin, C. Y. Huang, J. M. Chen, and R. G. Liu, *J. Solid State Chem.* **125**, 112 (1996); E. Pellegrin, L. H. Tjeng, F. M. F. de Groot, R. Hesper, G. A. Sawatzky, Y. Moritomo, and Y. Tokura, *J. Electron Spectrosc. Relat. Phenom.* **86**, 115 (1997).
- <sup>9</sup>T. A. Tyson, Q. Qian, C.-C. Kao, J.-P. Rueff, F. M. F. de Groot, M. Croft, S.-W. Cheong, M. Greenblatt, and M. A. Subramanian, *Phys. Rev. B* **60**, 4665 (1999).
- <sup>10</sup>G. Peng, F. M. F. de Groot, K. Hämäläinen, J. A. Moore, X. Wang, M. M. Grush, J. B. Hastings, D. P. Siddons, W. H. Armstrong, O. C. Mullins, and S. P. Cramer, *J. Am. Chem. Soc.* **116**, 2914 (1994), and references therein; R. D. Cowan, *The Theory of Atomic Structure and Spectra* (University of California Press, Berkeley, 1981); K. Tsutsumi, H. Nakamori, and K. Ichikawa, *Phys. Rev. B* **13**, 929 (1976) and references therein; see, for example, the case of Ti in *X-ray Spectroscopy*, edited by L. V. Azaroff (McGraw Hill, New York, 1974), p. 507; it should be noted that the peak normalization convention used here accentuates the very low intensity satellites of the higher valence spectra where the signal is low. In fact, in view of this, the discussion of the detailed variations in weak satellites of the higher valence spectra will be deferred to further work.
- <sup>11</sup>X. Wang, F. M. F. de Groot, and S. P. Cramer, *Phys. Rev. B* **56**, 4553 (1997).
- <sup>12</sup>F. M. F. de Groot, A. Fontaine, C.-C. Kao, and M. Krisch, *J. Phys.: Condens. Matter* **6**, 6875 (1994).
- <sup>13</sup>H. Chiba, M. Kikuchi, K. Kusuba, Y. Muraoka, and Y. Syono, *Solid State Commun.* **99**, 499 (1996).
- <sup>14</sup>C.-C. Kao, K. Hämäläinen, M. Krisch, D. P. Siddons, T. Overstuiizen, and J. B. Hastings, *Rev. Sci. Instrum.* **66**, 1699 (1995).
- <sup>15</sup>P. A. Lee, P. H. Citrin, P. Eisenberger, and B. M. Kincaid, *Rev. Mod. Phys.* **53**, 769 (1981).
- <sup>16</sup>T. A. Tyson (unpublished); *Phys. Rev. B* **49**, 12 578 (1994).
- <sup>17</sup>T. A. Tyson, K. O. Hodgson, C. R. Natoli, and M. Benfatto, *Phys. Rev. B* **46**, 5997 (1992).
- <sup>18</sup>Z. Mikic and E. C. Morse, *J. Comput. Phys.* **61**, 154 (1985); P. E. S. Wormer, F. Visser, and J. Paldus, *ibid.* **48**, 23 (1982); K. V. Vasavada and J. H. Freed, *Comput. Phys.* **3**, 61 (1989).
- <sup>19</sup>T. A. Tyson and C. R. Natoli (unpublished).
- <sup>20</sup>H. Woo, T. A. Tyson, M. Croft, S.-W. Cheong, and J. Woicik, *Phys. Rev. B* **63**, 134412 (2001).
- <sup>21</sup>P. F. Farges, G. E. Brown, Jr., and J. J. Rehr, *Phys. Rev. B* **56**, 1809 (1997).
- <sup>22</sup>K. R. Poeppelmeier, M. E. Leonowicz, J. C. Scanlon, J. M. Longo, and W. B. Yelon, *J. Solid State Chem.* **45**, 71 (1982).
- <sup>23</sup>J. Rodriguez-Carvajal, M. Hennion, F. Moussa, A. H. Moudden, L. Pinsard, and A. Revcolevschi, *Phys. Rev. B* **57**, R3189 (1998).
- <sup>24</sup>S. Satpathy, Z. Popovic, and F. Vukajlovic, *Phys. Rev. Lett.* **76**, 960 (1996).
- <sup>25</sup>F. Bridges, C. H. Booth, G. H. Kwei, J. J. Neumeier, and G. A. Sawatzky, *Phys. Rev. B* **61**, R9237 (2000).
- <sup>26</sup>Q. Qian, T. A. Tyson, C.-C. Kao, M. Croft, S.-W. Cheong, and M. Greenblatt, *Phys. Rev. B* **62**, 13 472 (2000).
- <sup>27</sup>Q. Huang, A. Santoro, J. W. Lynn, R. W. Erwin, J. A. Borchers, J. L. Peng, and R. L. Greene, *Phys. Rev. B* **55**, 14 987 (1997).
- <sup>28</sup>J. A. Alonso, M. J. Martinez-Lope, M. T. Casais, and M. T. Fernandez-Diaz, *Inorg. Chem.* **39**, 917 (2000).